

The S -matrix for surface boundary states: an application to photoemission for Weyl semimetals

D. Schmeltzer

*Physics Department, City College of the City University
of New York, New York, New York 10031, USA*

Abstract

We present a new theory of photoemission for Weyl semimetals. We derive this theory using a model with a boundary surface at $z = 0$. Due to the boundary, the self adjoint condition needs to be verified in order to ensure physical solutions. The solutions are given by two chiral zero modes which propagate on the boundary. Due to the Coulomb interaction, the chiral boundary model is in the same universality class as interacting graphene. The interactions cause a temperature dependence of the velocity and and life time. Using the principle of minimal coupling, we identify the electron-photon Hamiltonian. The photoemission intensity is computed using the S -matrix formalism. The S -matrix is derived using the initial photon state, the final state of a photoelectron and a hole in the valence band. The photoemission reveals the final valence band dispersion $\hbar v(\pm k_y - k_0) + \hbar\Omega$ after absorbing a photon of frequency Ω (k_0 represents the shift in the momentum due to the crystal potential). The momentum in the z direction is not conserved, and is integrated out. As a result, the scattering matrix is a function of the parallel momentum . We observe two dimensional contours, representing the "Fermi arcs", which for opposite spin polarization have opposite curvature. This theory is in agreement with previous experimental observations.

I. INTRODUCTION

Photoemission is the standard method used to provide information on the band structure in metals [1]. No such theory exists for the Weyl semimetal where the low energy electrons couple to photons via $\vec{\sigma} \cdot \vec{A}$ in the presence of a boundary at $z = 0$. The presence of the boundary demands special considerations [2].

Weyl fermions represent a pair of particles with opposite chirality, described by the massless solution of the Dirac equation [3]. Recently, it has been proposed that in materials with two non-degenerate bands crossing at the Fermi level in three dimensional ($3D$) momentum space, the low energy excitations can be described by the Weyl equations, allowing a condensed matter realization of Weyl fermion quasiparticles [4, 5]. The band crossing points are called Weyl points, and materials possessing such Weyl points are known as Weyl semimetals ($WSMs$). The bulk of the $WSMs$ is dominated by Weyl points with linear, low energy excitations. The Weyl points come in pairs with opposite chirality [6]. The surface state of the $WSMs$ is characterized by "Fermi arcs" that link the projection of the bulk Weyl points in the Brillouine zone. In the presence of parallel electric and magnetic fields, the $WSMs$ have a large negative magnetoresistance [7], due to the Adler-Bell-Jackiw chiral anomaly [8]. The $WSMs$ exist in materials where time-reversal symmetry or inversion are broken [4]. Recently, the non-centrosymmetric and non-crystal magnetic transition-metal monoarsenide/posphides $TaAs$, TaP , $NbAs$ and NbP have been predicted to be $WSMs$ with 12 pairs of Weyl points [9] as demonstrated by photoemission [10], scanning tunneling microscopy [11] and measurements of the quasiparticle profile [12, 13]. In contrast to the large amount of work devoted to photoemission experiments, few theoretical results exist for Weyl materials [14].

The early photoemission theories formulated by [1] and applications to experiments [15] were based on the matrix element $\vec{A} \cdot \vec{p} \approx \vec{A} \cdot i \frac{\vec{\nabla} V(\vec{x})}{\Omega}$ between the wave functions with the crystal potential $V(\vec{x})$ and the free space (where Ω is the laser frequency). In a regular metal, the dispersion of the electrons is approximately the same in the crystal and the vacuum. The only difference is the crystal potential, which is zero outside the crystal. As a result, the scattering problem involves the matrix element introduced by the crystal. Such a calculation is probably not possible for a Weyl semimetal where the $\vec{A} \cdot \vec{p}$ is not valid. The potential that describes the transition from free electrons to Dirac electrons with nodal points is not

available. Moreover, the presence of a boundary further complicates the problem. For a Dirac operator, the self-adjointing conjugation is not automatically satisfied, and according to [2], the boundary condition constrains the solutions.

We present a new theory which takes into consideration the boundary condition and the Dirac dispersion. This will be done using a non-linear model for *WSM* with two Weyl points restricted to the region $z < 0$ and a free electron system in the region $z > 0$. In the region $z < 0$ the Hamiltonian is built from two terms $h(\vec{k}, z) = h_0(\vec{k}, z) + h^\perp(\vec{k})$. $h_0(\vec{k}, z)$ contains the nonlinear part and the surface at $z=0$. The second term, $h^\perp(\vec{k})$, is z -independent with the momentum \vec{k} parallel to the surface $z = 0$. The parallel momentum of the emitted free electrons is equal to the parallel momentum of *WSM* electrons, the k_z component is not conserved and is integrated out, leaving only the conserved momentum \vec{k} . This Hamiltonian is time-reversal invariant and has broken inversion symmetry resulting in a model with a monopole-anti-monopole pair. The combination of the boundary condition and the Weyl nodes gives rise to a set of zero modes for the Hamiltonian $h_0(\vec{k}, z)$. The maximal amplitude to find an electron on the surface at $z = 0$ is obtained for zero mode spinors. The term $h^\perp(\vec{k})$ gives rise in the second quantized form to the Hamiltonian H^\perp with two chiral modes.

For $z > 0$, the model is given by the free electron $f_\sigma(\vec{k}, z)$, $f_\sigma^\dagger(\vec{k}, z)$ operator with the parabolic energy dispersion $E(\vec{k}, k_z)$. To ensure the continuity of the wave function from the bulk to the free space, we will introduce the interface Hamiltonian $H^{(interface)}$. The interface Hamiltonian describes the region between the bulk electrons and the free space electrons and has a width d around $z = 0$.

In the presence of the photon field \vec{A} , the Hamiltonian H^\perp is replaced by $H_0^\perp + H_{A_y}^\perp$ where $H_{A_y}^\perp$ is the photon Weyl-semimetal coupling. The photoemission scattering Hamiltonian $H_{int.}^{ext.}$ is built from the interface and the photon-Weyl coupling: $H_{int.}^{ext.} = H_{A_y}^\perp + H^{(interface)}$.

The Hamiltonian $H_{int.}^{ext.}$ allows us to compute the S -matrix [16] where the incoming state $|i\rangle$ scatters to an outgoing state $|f\rangle$. The matrix $S_{f,i}$ is given by:

$$outgoing\langle f|i\rangle_{incoming} = \langle f|T\left[e^{-\frac{i}{\hbar}\int_{-\infty}^{\infty} dt' H_{int.}^{ext.}(t')}\right]|i\rangle = S_{f,i}$$

When the initial state $|i\rangle$ is an incoming photon, the transition to the final state $|f\rangle$ is represented by the outgoing emitted electrons and a hole with a specific chirality is excited in the valence band. The formalism will be used to determine the valence band and conduction band dispersion and to demonstrate the presence of the "Fermi arcs". Due to the change in

chirality when we cross the point $k_x = \pm M$, the arcs for spin down electrons have opposite curvature to the ones with the spin up electrons .

Relaxation effects are considered in section VI where Coulomb interactions are considered.

In this paper we have obtained the following results:

- (a) We have obtained the chiral zero modes for the Weyl boundary Hamiltonian.
- (b) Using the minimal coupling principle, we have obtained the coupling between the photons and electrons.
- (c) Using the S -matrix formalism [16], we have obtained the intensity of the emitted photoelectrons from which the dispersion of the surface valence band was extracted.
- (d) Based on the the scattering matrix intensity, we have confirmed that the final valence band dispersion is $\epsilon = \hbar v(\pm k_y - k_0) + \hbar\Omega$, after absorbing the photon of frequency Ω . $-\hbar v k_0$ is the potential with respect to the outside crystal.
- (e) The photon absorption allows us to map the conduction band dispersion.
- (f) The momentum in the z direction is not conserved and is integrated out. This allows us to project the intensity into two dimensional contours and observe the "Fermi arcs" .
- (g) The change in chirality when we cross the nodal points $k_x = \pm M$ determines the curvature of the arcs. For spin down electrons, the curvature of the arcs is opposite to the one with spin up electrons.
- (h) Inclusion of the Coulomb interaction shows that the chiral zero modes which propagate on the boundary are in the same universality class as interacting graphene. As a result, the velocity and the life time become temperature -dependent.
- (k) This theory is in agreement with the experimental observation [10].

The paper is structured as follows. In Sec.II we present the WSM model and discuss the chiral zero modes resulting from the boundary conditions. Sec.III is devoted to the identification of the solid vacuum interface Hamiltonian. In Sec.IV and in Appendix A we study the detection of photoelectrons. In chapter V we present our photoemission results and compare them with the results given in the literature. Coulomb interactions are considered in section VI and Appendix B. Sec.VII is devoted to conclusions.

.

II. The Weyl Hamiltonian with a boundary at $z = 0$ confined to the crystal

region $-L \leq z \leq 0$

A WSM model without a boundary and two nodes $\vec{M} = [\pm M, 0, 0]$ is given by the Hamiltonian:

$$\tilde{H} = \int d^3x \hbar v \left[\hat{\Psi}_R^\dagger(\vec{x}) \vec{\sigma} \cdot \left(-i\vec{\partial} - \vec{M} \right) \hat{\Psi}_R(\vec{x}) - \hat{\Psi}_L^\dagger(\vec{x}) \vec{\sigma} \cdot \left(-i\vec{\partial} - (-\vec{M}) \right) \hat{\Psi}_L(\vec{x}) \right] \quad (1)$$

We observe that the Hamiltonian in Eq.(1) describes fermions with opposite chirality and two singularities at $k_x = \pm M$. This model is oversimplified and does not include the band dispersion which connects the two nodes. In order to observe this connection we need to study a model with two non-linearly dispersed bands. We are guided by the fact that the singularities at $k_x = \pm M$ describe a monopole and anti-monopole. The monopole-anti-monopole is present when one of the symmetries, time reversal or inversion symmetry, is broken. To describe the crossing of the bands in momentum space, we will introduce a quadratic function of momentum $g(k_x^2 - M^2)$ which reproduces the nodes at $\pm M$ (this polynomial is obtained by replacing $-\cos(k_x) + 1 \approx \frac{k_x^2}{2}$) for the two band Hamiltonian $\hat{h}(\vec{k}, z)$: $\hat{h}(\vec{k}, z) = \hbar v \left[\sigma_y \tau_3 k_y + \sigma_z \tau_3 k_z + \sigma_y \tau_2 g(k_x^2 - M^2) \right]$.

This Hamiltonian is invariant with respect to the time-reversal symmetry and has a broken inversion symmetry. As a result, $k_x = \pm M$ is a monopole-anti-monopole pair.

Next, we introduce a Hamiltonian with a boundary surface at $z = 0$. This is obtained by replacing the momentum k_z with $-i\partial_z$ and restricting the space to $-L \leq z \leq 0$ where the potential of the crystal with respect to the vacuum is given by $-V_0$. We use the notation $-V_0 = -\hbar v k_0$ for the $z \leq 0$ region and $k_0 = 0$ for $z > 0$. The Hamiltonian with the boundary at $z = 0$ is given by:

$$\begin{aligned} H &= \int \frac{d^2k}{(2\pi)^2} \int_{-L}^0 dz \left[\hbar v \hat{\Psi}^\dagger(\vec{k}, z) \left(\sigma_y \tau_3 k_y + \sigma_z \tau_3 (-i\partial_z) + \sigma_y \tau_2 g(k_x^2 - M^2) - k_0 \right) \hat{\Psi}(\vec{k}, z) \right] \\ &= \int \frac{d^2k}{(2\pi)^2} \int_{-L}^0 dz \left[\hbar v \hat{\Psi}^\dagger(\vec{k}, z) h(\vec{k}, z) \hat{\Psi}(\vec{k}, z) \right] \end{aligned} \quad (2)$$

The Hamiltonian in Eq.(2) consists of two orbitals described by the Pauli matrices τ_1, τ_2 and τ_3 . The spin of the electrons is introduced with the help of the Pauli matrices σ_x, σ_y and σ_z . The translation symmetry along the y direction is preserved, so that k_y is a good quantum number. For the semi-infinite system in Eq.(2), we need to check if the Dirac operator with

the boundary term $\sigma_z \tau_3 (-i\partial_z)$ has real eigenvalues. We apply the division described in [18] to the the Hamiltonian $h(\vec{k}, z)$:

$$\begin{aligned} h(\vec{k}, z) &= h_0(\vec{k}, z) + h^\perp(\vec{k}) \\ h_0(\vec{k}, z) &= \hbar v \left[\sigma_z \tau_3 (-i\partial_z) + \sigma_y \tau_2 g(k_x^2 - M^2) \right] \\ h^\perp(\vec{k}) &= \hbar v \left[\sigma_y \tau_3 k_y - k_0 \right] \end{aligned} \tag{3}$$

In the region $-L \leq z \leq 0$, the Hamiltonian $h_0(\vec{k}, z)$ obeys the eigenvalue equation:

$$\left[\sigma_z \tau_3 (-i\partial_z) + \sigma_y \tau_2 g(k_x^2 - M^2) \right] U(\vec{k}, z) = EU(\vec{k}, z), \quad -L \leq z \leq 0 \tag{4}$$

The eigenvector $U(\vec{k}, z)$ is a function of the momentum \vec{k} parallel to the surface $z = 0$. For the eigenvector $U(\vec{k}, z)$, we seek a solution of form $U(\vec{k}, z) = e^{\lambda z} V(\vec{k})$ and find the eigenvalues $E = \pm \sqrt{\lambda^2 - (g(k_x^2 - M^2))^2}$. The self-adjointing condition [2] is satisfied for real eigenvalues E . The condition for real eigenvalues E is equivalent with $\lambda^2 > (g(k_x^2 - M^2))^2$. Since the electrons are confined to the region $-L \leq z \leq 0$, only solutions with positive λ are acceptable in the limit $L \rightarrow \infty$ (the normalization of the wave function $U(\vec{k}, z)$ demands that λ obeys the condition $\lambda z < 0$, while negative values of λ are excluded in the limit $L \rightarrow \infty$). Using the relationship between λ and the eigenvalue E , we find that the amplitude of the wave function in the region $z \leq 0$ is given by $e^{\lambda z} = e^{\sqrt{E^2 + (g(k_x^2 - M^2))^2} z}$. Since E must be *real*, we determine that the maximal amplitude $e^{\lambda z}$ is achieved for zero mode solutions $E = 0$, resulting in the amplitude $e^{|g(k_x^2 - M^2)|z}$. As a result, the maximal amplitude of the wave function $U(\vec{k}, z)$ in the region $z \leq 0$ is given by the zero mode solution:

$$U(\vec{k}, z) = e^{\lambda z} V(\vec{k}) = \theta[k_x^2 - M^2] e^{g(k_x^2 - M^2)z} \eta_{i,+} + \theta[-k_x^2 + M^2] e^{-g(-k_x^2 + M^2)z} \eta_{i,-}(\vec{k}); \quad k^2 \neq M^2 \tag{5}$$

$\eta_{i,\pm}$, $i = 1, 2$ are the two zero mode spinors, the index \pm refers to the space region $k_x^2 > M^2$ and $M^2 > k_x^2$, respectively.

$$\begin{aligned} \eta_{1,+} &= \sqrt{\frac{1}{2}} [i, 0, 0, 1]^T, \quad \eta_{1,-} = \sqrt{\frac{1}{2}} [-i, 0, 0, 1]^T \\ \eta_{2,+} &= \sqrt{\frac{1}{2}} [0, i, 1, 0]^T, \quad \eta_{2,-} = \sqrt{\frac{1}{2}} [0, -i, 1, 0]^T \end{aligned} \tag{6}$$

This amplitude will contribute the most to the intensity of the emitted photoelectrons.

The fermion spinor $\hat{\Psi}(\vec{x}, z)$ is replaced by the projected zero mode spinor $\Psi(\vec{x}, z)$.

$$\Psi(\vec{x}, z) = \int \frac{d^2k}{(2\pi)^2} \sqrt{2\hat{g}s(k_x)} e^{\hat{g}s(k_x)z} e^{i\vec{k}\cdot\vec{x}} \sum_{i=1,2} \sum_{s=\pm} C_{i,s}(\vec{k}) \alpha_s(k_x) \eta_{i,s}, \quad k_x^2 \neq M^2 \quad (7)$$

The spinor is normalized in the region $[-L, 0]$. This gives rise to the factor $\sqrt{2\hat{g}s(k_x)}$, where the exponent originate from the zero mode Eq.6. The notation $\alpha_{s=1}(k_x) \equiv \theta[k_x^2 - M^2]$ is the step function which is 1 for $k_x^2 - M^2 > 0$ and zero for $k_x^2 - M^2 < 0$. Similarly, $\alpha_{s=-1}(k_x) \equiv \theta[(-k_x^2 + M^2)]$ is 1 for $M^2 - k_x^2 > 0$ and zero for $M^2 - k_x^2 < 0$. We simplify the notation in Eq.(5), $g|[(k_x^2 - M^2)] \equiv \hat{g}s(k_x)$ where $s(k_x)$ and \hat{g} are given by, $s(k_x) = |[(\frac{k_x}{M})^2 - 1]|$, $\hat{g} = gM^2$, respectively.

Using the spinor representation given in Eq.(7), we diagonalize the Hamiltonian $h^\perp(\vec{k})$. In the presence of the photon field $\vec{A}(\vec{x})$, we obtain:

$$\begin{aligned} H^\perp &= H_0^\perp + H_{A_y}^\perp = \int \frac{d^2k}{(2\pi)^2} \int_{-L}^0 dz \hbar v \Psi^\dagger(\vec{k}, z) h^\perp(k_y - A_y) \Psi(\vec{k}, z) \\ H_0^\perp &= \int \frac{d^2k}{(2\pi)^2} \sum_{\pm} \hbar v \left[k_y \left(-iC_{1,s}^\dagger(\vec{k}) C_{2,s}(\vec{k}) \alpha_s(k_x) + iC_{2,s}^\dagger(\vec{k}) C_{1,s}(\vec{k}) \alpha_s(k_x) \right) \right. \\ &\quad \left. - k_0 \left(C_{1,s}^\dagger(\vec{k}) C_{1,s}(\vec{k}) \alpha_s(k_x) + C_{2,s}^\dagger(\vec{k}) C_{2,s}(\vec{k}) \alpha_s(k_x) \right) \right] \\ H_{A_y}^\perp &= \sum_{s=\pm} \int \frac{d^2k}{(2\pi)^2} W(k_x, \vec{q}) A_y(\vec{q}, t) \left[iC_{1,s}^\dagger(\vec{k}) C_{2,s}(\vec{k} + \vec{q}) \alpha_s(k_x + q_x) - iC_{2,s}^\dagger(\vec{k}) C_{1,s}(\vec{k} + \vec{q}) \alpha_s(k_x + q_x) \right] \\ W(k_x, \vec{q}) &= \frac{2\hat{g}s(k_x) e^{-itan^{-1}(\frac{q_z}{2\hat{g}s(k_x)})}}{\sqrt{(2\hat{g}s(k_x))^2 + q_z^2}} \end{aligned} \quad (8)$$

where \vec{q} is the photon momentum and $\Omega(\vec{q})$ is the photon frequency. We introduce chiral operators $C_{R,s}(\vec{k})$, $C_{L,s}(\vec{k})$ and find the two eigenvalues $\pm k_y - k_0$:

$$C_{1,s}(\vec{k}) = \frac{1}{\sqrt{2}} \left(C_{R,s}(\vec{k}) + C_{L,s}(\vec{k}) \right); \quad C_{2,s}(\vec{k}) = \frac{i}{\sqrt{2}} \left(C_{R,s}(\vec{k}) - C_{L,s}(\vec{k}) \right) \quad (9)$$

In the chiral representation, the Hamiltonian H^\perp takes the form:

$$\begin{aligned} H_0^\perp &= \int \frac{d^2k}{(2\pi)^2} \sum_{s=\pm} \left[\hbar v (k_y - k_0) C_{R,s}^\dagger(\vec{k}) C_{R,s}(\vec{k}) \alpha_s(k_x) + \hbar v (-k_y - k_0) C_{L,s}^\dagger(\vec{k}) C_{L,s}(\vec{k}) \alpha_s(k_x) \right] \\ H_{A_y}^\perp &= \sum_{s=\pm} \int \frac{d^2k}{(2\pi)^2} W(k_x, \vec{q}) A_y(\vec{q}, t) \left[C_{L,s}^\dagger(\vec{k}) C_{L,s}(\vec{k} + \vec{q}) \alpha_s(k_x + q_x) - C_{R,s}^\dagger(\vec{k}) C_{R,s}(\vec{k} + \vec{q}) \alpha_s(k_x + q_x) \right] \end{aligned} \quad (10)$$

In Eq.(10) we observe that the right chiral electrons have the band dispersion $\hbar v(k_y - k_0)$ and the left chiral electrons have the band dispersion $\hbar v(-k_y - k_0)$.

In the next stage, we will replace the chiral operators $C_{R,s}(\vec{k})$, $C_{L,s}(\vec{k})$ with the particle $a_{R,s}(\vec{k})$, $a_{L,s}(\vec{k})$ and anti-particle operators $b_{R,s}^\dagger(-\vec{k})$, $b_{L,s}^\dagger(-\vec{k})$ where $\theta[k_y] = 1$ for $k_y \geq 0$:

$$\begin{aligned} C_{R,s}(\vec{k}) &= \theta[k_y] \alpha_s(k_x) a_{R,s}(\vec{k}) + \theta[-k_y] \alpha_s(k_x) b_{R,s}^\dagger(-\vec{k}) \\ C_{L,s}(\vec{k}) &= \theta[-k_y] \alpha_s(k_x) a_{L,s}(\vec{k}) + \theta[k_y] \alpha_s(k_x) b_{L,s}^\dagger(-\vec{k}) \end{aligned} \tag{11}$$

This allows us to replace the chiral bands in Eq.(10) and introduce for the boundary surface the *valence* and *conduction* bands. The representation in Eq.(11) is essential for the use of the Wick theorem [16] which relies on the property that the operators for the particles $a_{R,s}(\vec{k})$, $a_{L,s}(\vec{k})$ and anti-particle $b_{R,s}(-\vec{k})$, $b_{L,s}(-\vec{k})$ annihilate the ground state.

III. The vacuum solid interface Hamiltonian

In the next section we present the vacuum-solid interface Hamiltonian. At the interface $z = 0$ we have a region of width d where both H^\perp and $H^{(vacuum)}$ are valid. $H^{(vacuum)}$ is given by:

$$\begin{aligned} H^{(vacuum)} &= \int \frac{d^2 k}{(2\pi)^2} \int_0^\infty \frac{dk_z}{\pi} \sum_{\sigma=\uparrow,\downarrow} \left[E(\vec{k}, k_z) f_\sigma^\dagger(\vec{k}, k_z) f_\sigma(\vec{k}, k_z) \right], E(\vec{k}, k_z) = E(\vec{k}, 0) + \Delta; \\ E(\vec{k}) &= \frac{\hbar^2 |\vec{k}|^2}{2m}, \Delta = \frac{\hbar^2 k_z^2}{2m} \end{aligned} \tag{12}$$

$H^{(vacuum)}$ is given in terms of the electron operators $f_\sigma(\vec{k}, z)$, $f_\sigma^\dagger(\vec{k}, z)$, and a parabolic energy dispersion $E(\vec{k}, k_z) = E(\vec{k}, 0) + \Delta$ in the the region $[0, L]$. The dispersion $E(\vec{k}, 0)$ represents the energy of the emitted electrons given as a function of the parallel conserved momentum \vec{k} . The z component of the momentum is integrated out. The z -dependent energy is given by $\Delta = \frac{\hbar^2 k_z^2}{2m}$. The interface Hamiltonian is controlled by the vacuum solid potential $-V_0(z)$, which changes from zero outside the crystal to $-V_0$ inside the crystal. The interface Hamiltonian is approximated by a smooth function of the form $(e^{\kappa(z-d)} - 1)V_0$. At $z = d$ the potential is zero and for $z = -L$ the potential is $-V_0$:

$$\begin{aligned}
H^{(interface)} = & \int_{-L}^d dz \int d^2x \sum_{\sigma=\uparrow,\downarrow} f_{\sigma}^{\dagger}(\vec{x}, z) \left(e^{\kappa(z-d)} - 1 \right) V_0 \Psi(\vec{x}, z) + h.c. = \int_0^{\infty} \frac{dk_z}{\pi} \int \frac{d^2k}{(2\pi)^2} S(\vec{k}, k_z; \kappa) V_0 \cdot \\
& \left[f_{\uparrow}^{\dagger}(\vec{k}, k_z) \left(\frac{\alpha_+(k_x)}{\sqrt{2}} (iC_{1,+}(\vec{k}) + C_{2,+}(\vec{k})) + \frac{\alpha_-(k_x)}{\sqrt{2}} (-iC_{1,-}(\vec{k}) + C_{2,-}(\vec{k})) \right) \right. \\
& \left. + f_{\downarrow}^{\dagger}(\vec{k}, k_z) \left(\frac{\alpha_+(k_x)}{\sqrt{2}} (C_{1,+}(\vec{k}) + iC_{2,+}(\vec{k})) + \frac{\alpha_-(k_x)}{\sqrt{2}} (C_{1,-}(\vec{k}) - iC_{2,+}(\vec{k})) \right) + h.c. \right] = \\
& \int_0^{\infty} \frac{dk_z}{\pi} \int \frac{d^2k}{(2\pi)^2} S(\vec{k}, k_z; \kappa) V_0 \left[i f_{\uparrow}^{\dagger}(\vec{k}, k_z) \left(\alpha_+(k_x) C_{R,+}(\vec{k}) - \alpha_-(k_x) C_{L,-}(\vec{k}) \right) + \right. \\
& \left. f_{\downarrow}^{\dagger}(\vec{k}, k_z) \left(-\alpha_+(k_x) C_{L,+}(\vec{k}) + \alpha_-(k_x) C_{R,-}(\vec{k}) \right) + h.c. \right]
\end{aligned} \tag{13}$$

where the integration with respect z introduces the function $S(\vec{k}, k_z; \kappa)$ which describes the interface: $S(\vec{k}, k_z; \kappa) = \int_{-L}^0 dz \sqrt{2\hat{g}(s(k_x))} \left[e^{i(k_z + \hat{g}(s(k_x))z)} \cdot (e^{\kappa z} - 1) \right]$. In obtaining Eq.(13), the fermion $f_{\sigma}(\vec{k}, z)$ is replaced by a spinor with two spin components and two orbitals. For the free electrons we will choose the spinor representations $f_{\sigma=\uparrow} \rightarrow [1, 0, 1, 0]^T$ and $f_{\sigma=\downarrow} \rightarrow [0, 1, 0, 1]^T$. The term $S(\vec{k}, k_z; \kappa)$ depends on the parallel momentum \vec{k} and the $k_z > 0$ momentum which is a function of the energy Δ .

IV. The detection of photoelectrons

The vector potential for a photon field of frequency Ω is given by $\vec{A}(\vec{x}, t) = \vec{e}_r(\vec{q}) \frac{A_r(\vec{q})}{\sqrt{2\Omega(\vec{q})}} e^{i\vec{q}\cdot\vec{x}} e^{-i\Omega t} + \vec{e}_r(\vec{q}) \frac{A_r^{\dagger}(\vec{q})}{\sqrt{2\Omega(\vec{q})}} e^{-i\vec{q}\cdot\vec{x}} e^{i\Omega t}$. The photons propagate in the direction $\frac{\vec{q}}{|\vec{q}|} = [\sin(\theta) \cos(\phi), \sin(\theta) \sin(\phi), \cos(\theta)]$ with respect to the sample surface. The photon field has two orthogonal polarizations to $\frac{\vec{q}}{|\vec{q}|}$ which are given by $\vec{e}_r(\vec{q})$, $r = 1, 2$. The vector potential $\vec{A}(\vec{x}, t)$ corresponds to a single photon of frequency Ω and momentum \vec{q} .

In order to compute the intensity of the emitted photoelectrons, we need to identify the scattering Hamiltonian $H_{int.}^{ext.}$ responsible for the photoemission. $H_{int.}^{ext.}$ is the sum of the interface Hamiltonian $H^{(interface)}$ given in Eq.(13) and the $H_{A_y}^{\perp}$ Hamiltonian given in Eq.(8).

$$H_{int.}^{ext.} = H^{(interface)} + H_{A_y}^{\perp} \tag{14}$$

From the Hamiltonian $H_{int.}^{ext.}$ we obtain the S -matrix. The scattering matrix is defined as

a process where an incoming state $|i\rangle$ scatters to an outgoing state $|f\rangle$. We represent this process as:

$$\text{outgoing}\langle f|i\rangle_{\text{incoming}} = S_{f,i} = \langle f|T\left[e^{-\frac{i}{\hbar}\int_{-\infty}^{\infty} dt' H_{\text{int.}}^{\text{ext.}}(t')}\right]|i\rangle \quad (15)$$

The S -matrix is given as a time order product (T) that acts on the initial state $|i\rangle$ and final state $|f\rangle$ [16]. In a photoemission experiment incoming photons produce outgoing electrons. The S matrix for an incoming photon and an outgoing electron only is zero. If the emitted electron is accompanied by an internal excitation, the S matrix is finite. When the *initial* state $|i\rangle$ is a single photon of frequency Ω and polarization r , $|i\rangle = A_r^\dagger(\vec{q})|0\rangle$, and the outgoing electron is accompanied by a hole excitation in the valence band, at the second order in $H_{\text{int.}}^{\text{ext.}}$ we find a finite S matrix. The Hamiltonian $H_{\text{int.}}^{\text{ext.}}$ allows for two chiral states for the hole operators and two spin polarizations of the emitted electrons. When the final state $|\chi\rangle$ is unknown, the scattering amplitude is represented by $S_{\chi,i}$, which is approximated by $S_{f^{(L,\sigma)},i}$, $S_{f^{(R,\sigma)},i}$ or the non-relativistic amplitude $S_{f^{(\text{parabolic},\sigma)},i}$. A good approximation satisfies $|S_{\chi,i}|^2 \approx \sum_{\sigma\uparrow,\downarrow} \left(|S_{f^{(R,\sigma)},i}|^2 + |S_{f^{(L,\sigma)},i}|^2 + |S_{f^{(\text{parabolic},\sigma)},i}|^2 \right)$ (see the discussions in the next section).

The final states $|f^{(R,\sigma)}\rangle$ and $|f^{(L,\sigma)}\rangle$ are given by:

$$\begin{aligned} |f^{(R,\uparrow)}\rangle &= \sum_{s=1,-1} \left[f_{\sigma=\uparrow}^\dagger(\vec{p}, p_z) b_{R,s}^\dagger(-\vec{p}) \alpha_s(p_x) \theta[-p_y] \right] |0\rangle \\ |f^{(R,\downarrow)}\rangle &= \sum_{s=1,-1} \left[f_{\sigma=\downarrow}^\dagger(\vec{p}, p_z) b_{R,s}^\dagger(-\vec{p}) \alpha_s(p_x) \theta[-p_y] \right] |0\rangle \\ |f^{(L,\uparrow)}\rangle &= \sum_{s=1,-1} \left[f_{\sigma=\uparrow}^\dagger(\vec{p}, p_z) b_{L,s}^\dagger(-\vec{p}) \alpha_s(p_x) \theta[p_y] \right] |0\rangle \\ |f^{(L,\downarrow)}\rangle &= \sum_{s=1,-1} \left[f_{\sigma=\downarrow}^\dagger(\vec{p}, p_z) b_{L,s}^\dagger(-\vec{p}) \alpha_s(p_x) \theta[p_y] \right] |0\rangle \end{aligned} \quad (16)$$

We first consider the case in which the final state is $|f^{(L,\sigma)}\rangle$ and obtain information on the valence band dispersion $\hbar v(-k_y - k_0)$. Choosing $|f^{(R,\sigma)}\rangle$, we will obtain the information for the band $\hbar v(k_y - k_0)$. To compute the matrix element $S_{f^{(L,\sigma)},i}$ for the initial photon state $|i\rangle = A_r^\dagger(\vec{q})|0\rangle$ and final state $|f^{(L,\sigma)}\rangle$ we use Eq.(16). The second order in $H_{\text{int.}}^{\text{ext.}}$ gives the amplitude $S_{f^{(L,\sigma)},i}$:

$$S_{f^{(L,\sigma=\uparrow)},i} = \left(\frac{-i}{\hbar}\right)^2 \int_{-\infty}^{\infty} dt \int_{-\infty}^{\infty} dt' \langle 0(f^{(L,\sigma=\uparrow)})^\dagger | T \left[H_{\text{int.}}^{\text{ext.}}(t) H_{\text{int.}}^{\text{ext.}}(t') \right] A_r^\dagger(\vec{q}) | 0 \rangle$$

$$S_{f^{(L,\sigma=\downarrow)},i} = \left(\frac{-i}{\hbar}\right)^2 \int_{-\infty}^{\infty} dt \int_{-\infty}^{\infty} dt' \langle 0 | (f^{(L,\sigma=\downarrow)})^\dagger | T \left[H_{int}^{ext.}(t) H_{int}^{ext.}(t') \right] A_r^\dagger(\vec{q}) | 0 \rangle \quad (17)$$

The Wick theorem reduces the T -product to a product of contractions (given by Green's function), then it acts on the uncontracted fields on the initial state $|i\rangle = A_r^\dagger(\vec{q})|0\rangle$ and final state $\langle f^{(L,\sigma)}|$. The computation of the matrix element $S_{f^{(L,\sigma=\uparrow)},i}$ is given in *Appendix A*.

The result of the Wick theorem for the final state, $\langle f^{(L,\sigma)}|$ is: one photon is absorbed, one electron is created in the conduction band and a hole is excited in the valence band. The result for the matrix element $S_{f^{(L,\uparrow)},i}$ in Eq.(18) is a function of the emitted electron energy $E(\vec{k}, k_z)$. The information regarding the quasi-particle excitation is obtained from the free electrons which have a finite amplitude to propagate into the region $z > 0$ with the same parallel momentum and the energy $E(\vec{k}, 0)$. The integration with respect to the momentum k_z replaces the valence electron energy with $E(\vec{k}, 0)$ plus an average with respect to $\Delta(k_z)$:

$$S_{f^{(L,\uparrow)},i} \propto \left(\frac{-i}{\hbar}\right)^2 \int_0^\infty \frac{dk_z}{\pi} M(\vec{k}, k_z, \vec{q}, \kappa) \theta[-k_y] \theta[k_y + q_y] \theta[M^2 - k_x^2] \cdot \frac{-i}{\left(E(\vec{k}, 0) + \Delta(k_z) - \hbar v(k_y + k_0) \theta[-k_y]\right)} \cdot \delta \left[E(\vec{k}, 0) + \Delta(k_z) + \hbar v(k_y + q_y + k_0) \theta[k_y + q_y] - \hbar \Omega(\vec{q}) \right] \quad (18)$$

Here, the matrix element $M(\vec{k}, k_z, \vec{q}, \kappa)$ is given by the product of $W(\vec{k}, \vec{q})$ and $S(\vec{k}, k_z, \kappa)$ introduced in Eq.(8) and Eq.(13): $M(\vec{k}, k_z, \vec{q}, \kappa) = W(\vec{k}, \vec{q}) S(\vec{k}, k_z, \kappa) V_0 e_r^{(y)}(\vec{q})$. We perform the k_z integration, shift the momentum $k_y \rightarrow k_y - q_y$ and introduce the life time Γ . In Eq.(18) we replace $E(\vec{k} - q_y, 0) - \hbar \Omega(\vec{q})$ with ϵ and identify the valence electron energy, $\epsilon = E(\vec{k} - q_y, 0) - \hbar \Omega(\vec{q})$. Specifically, we find:

$$S_{f^{(L,\uparrow)},i} \propto \left(\frac{-i}{\hbar}\right)^2 M(\vec{k}, \Delta(\vec{k}), \vec{q}, \kappa) \theta[-k_y + q_y] \theta[k_y] \theta[M^2 - k_x^2] \cdot \frac{1}{\sqrt{\left(\epsilon + \hbar v(k_y + k_0) \theta[k_y] + i\Gamma\right)}} \cdot \frac{1}{\left(\hbar \Omega(\vec{q}) - \hbar v(k_y + q_y + k_0) + i\Gamma\right)} \quad (19)$$

This expression demonstrate that the amplitude $S_{f^{(L,\uparrow)},i}$ has information about the valence band dispersion $\epsilon = \hbar v(-k_y - k_0)$. Not shown is the amplitude $S_{f^{(R,\uparrow)},i}$ with the dispersion $\epsilon = \hbar v(k_y - k_0)$. In Eq.(19) we have introduced the life time Γ which is a result of electron-electron interactions (see section *VI*) or impurities scattering. The elastic

impurities scattering is less significant since the Hamiltonian H_0^\perp (Eq. 10) is time reversal invariant \hat{T} in two space dimensions, obeying the condition $\hat{T}^2 = -1$. Our model with a disorder potential belongs to the symplectic class which has no localized phase [21].

In section VI we consider the Coulomb interaction in the absence of impurities scattering. A number of authors have shown that at finite temperatures the impurity scattering mean free path $l_{imp.}$ can be larger than the electron-electron scattering mean free path l_{e-e} , $l_{e-e} < l_{imp.}$ [19]. As a result as observed in graphene, that the velocity v and the life time Γ renormalizes, becoming temperature dependent. It was shown [20] that at $T = 0$ the dispersion in graphene is anomalous therefore we expect similar feature for the Weyl semimetal.

V. Physical information obtained from the scattering matrix

In the literature, the computation of the optical Joint density of states involving the valence band and conduction band [13] provides information about energy dispersion. Our computation given in Eq.(19) reveals similar features. However, we have only one conduction and one valence band giving rise to a simplified picture, as a function of the photon frequency, shifted energy $\epsilon = E(\vec{k} - q_y, 0) - \hbar\Omega(\vec{q})$ and momentum \vec{k} .

In a photoemission experiment the experimentalist measures the energy of the emitted electrons $E_{em.}(\theta, \phi)$ as a function of the orientation of the crystal surface. From this energy and orientation (using the model of free electrons) we determine $E(\vec{k}, 0) = E_{em.}(\theta, \phi) \sin^2(\theta)$ and $\vec{k}(\theta, \phi)$. These results are used to determine the valence band energy given by $\epsilon = E(\vec{k}, 0) - \hbar\Omega(\vec{q}) = E_{em.}(\theta, \phi) \sin^2(\theta) - \hbar\Omega(\vec{q})$ used in Eq(19). We generate a plot of the experimental results and determine if the points (ϵ, \vec{k}) , fit the dispersion $\epsilon = \hbar v(-k_y - k_0)$, $\epsilon = \hbar v(k_y - k_0)$ or $\epsilon = \frac{\hbar^2}{2m}|\vec{k}|^2 - V_0$ (parabolic dispersion). In all these cases we need to consider the energy or temperature dependence of the life time Γ . The dispersion $\epsilon = \hbar v(-k_y - k_0)$ corresponds to the scattering amplitude $S_{f(L,\uparrow),i}$, the dispersion $\epsilon = \hbar v(k_y - k_0)$ corresponds to $S_{f(R,\uparrow),i}$ and the case $\epsilon = \frac{\hbar^2}{2m}|\vec{k}|^2 - V_0$ corresponds to a non-Dirac scattering amplitude $S_{f(parabolic,\sigma),i}$. The unknown scattering amplitude $S_{\chi,i}(\epsilon, \vec{k}) = \langle \chi | T \left[e^{-\frac{i}{\hbar} \int_{-\infty}^{\infty} dt' H_{int.}^{\epsilon \sigma t'}(t')} \right] | i \rangle$ for the final state $\langle \chi |$ obeys the relation $|S_{\chi,i}(\epsilon, \vec{k})|^2 \approx \sum_{\sigma=\uparrow,\downarrow} \left(|S_{f(L,\sigma),i}|^2 + |S_{f(R,\sigma),i}|^2 + |S_{f(parabolic,\sigma),i}|^2 \right)$.

Next, we analyze the situation for the chiral final states given in Eq.(16). We compute

$S_{f(L,\sigma),i}$ and find the following scattering intensity :

$$\begin{aligned}
& |S_{f(L,\uparrow),i} + S_{f(L,\downarrow),i}|^2 \approx \\
& \theta[-k_y + q_y]\theta[k_y] \frac{(2\hat{g}s(k_x))^2}{q_z^2 + (2\hat{g}s(k_x))^2} |M(\vec{k}, \Delta(\vec{k}), \vec{q}, \kappa)|^2 \frac{1}{\sqrt{((\epsilon + \hbar v(k_y + k_0)\theta[k_y])^2 + \Gamma^2)}} . \\
& \frac{1}{((\hbar\Omega(\vec{q}) - \hbar v(k_y + q_y + k_0))^2 + \Gamma^2)} \left[\delta_{\sigma=\uparrow}\theta[M^2 - k_x^2] + \delta_{\sigma=\downarrow}\theta[k_x^2 - M^2] \right]
\end{aligned} \tag{20}$$

We observe that the scattering amplitude $|S_{f(L,\sigma),i}|^2$ has two singularities . The first is given by the shifted valence band dispersion $\epsilon = \hbar v(-k_y - k_0)$ where $\epsilon = E(\vec{k} - q_y, 0) - \hbar\Omega(\vec{q})$, the second gives information on the conduction band and photon frequency $\hbar\Omega(\vec{q}) = \hbar v(k_y + k_0 - q_y)$. These results confirm that both the dispersion and the photon absorption from the valence to the conduction band can be obtained theoretically in agreement with the photoemission experiments.

Using the results given in Eq.(20), we plot the scattering intensity matrix. We will use the units of eV for the momentum k_y , k_0 and frequency Ω . The intensity $|S_{f(L,\sigma),i}|^2$ and the photon absorption are plotted in arbitrary units.

The scattering intensity $|S_{f(L,\uparrow),i}|^2(\epsilon)$ for a fixed momentum $k_x = 0$ and photon frequency $\Omega = 50\text{eV}$, reveals that the maximum intensity varies with the valence band energy ϵ and momentum k_y .

The scattering intensity $|S_{f(L,\sigma),i}|^2(k_x, k_y)$ is a function of the momentum k_x , k_y and shows evidence of the nodal points at $k_x = \pm 0.5$.

Figure 1 shows the scattering intensity $|S_{f(L,\sigma=\uparrow),i}|^2(k_y, \epsilon)$ for photoelectrons with spin $\sigma = \uparrow$ and left chirality for the valence band $\epsilon = \hbar v(-k_y - k_0)\theta[k_y]$. The intensity is a function of the momentum k_y and energy $\epsilon(\vec{k})$ for the photon frequency measured in eV., $\Omega = 100\text{eV}$. This figure reveals the dispersion $\epsilon = \hbar v(-k_y - k_0)$ for $k_y > 0$ of the valence band shifted by the laser frequency presented in the (ϵ, k_y) plane.

Figure 2 shows the scattering intensity $|S_{f(L,\sigma=\uparrow),i}|^2(k_y, \Omega)$ as a function of the photon frequency Ω and the momentum k_y . This figure reveals the conduction band dispersion due to the photon absorption $\hbar\Omega(\vec{q}) \approx \hbar v(k_y + k_0)$.

Figures 1 and 2 with the dispersion equation $\epsilon(\vec{k}) = \hbar v(-k_y - k_0)$ and $\hbar\Omega(\vec{q}) \approx \hbar v(k_y + k_0)$

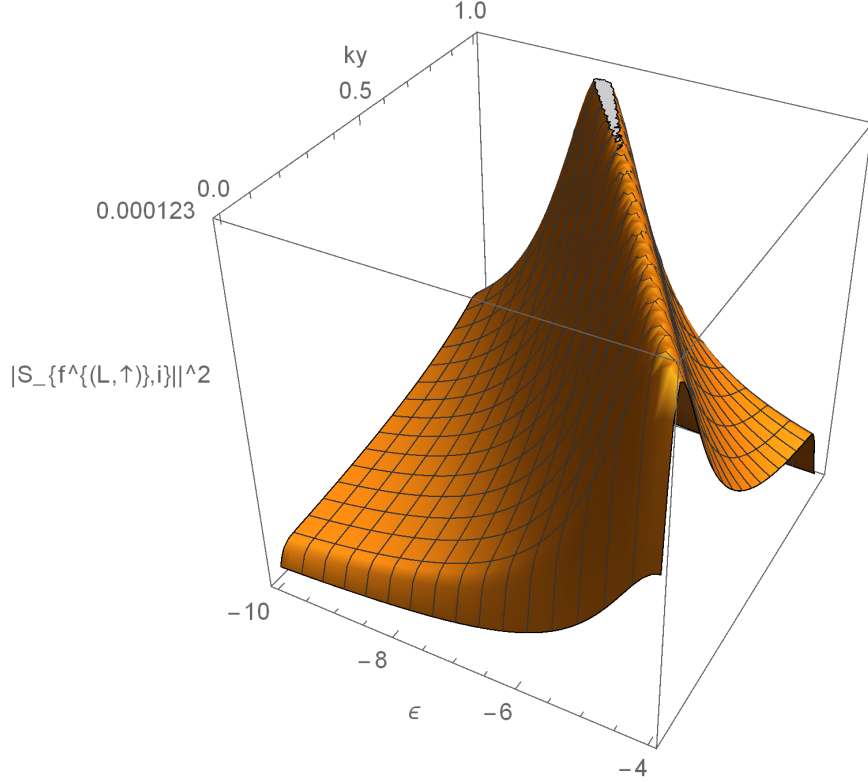


FIG. 1: The scattering intensity $|S_{f^{(L,\uparrow)},i}|^2(k_y, \epsilon)$ for dispersion $\epsilon = \hbar v(-k_y - k_0)\theta[k_y]$ ($\epsilon = E(k_y - q_y, k_x = 0) - \hbar\Omega(\vec{q})$). A life time Γ for the valence band ϵ was used in the plot. The confinement potential is $V_0 = 4ev$ and the photon frequency is $\Omega = 100ev$. The coordinates (x, y) corresponds to (k_y, ϵ) , the z axis is represented by $|S_{f^{(L,\uparrow)},i}|^2$ computed for a small value of the life time Γ .

are in agreement with the experimental observations [10].

Figure 3 shows the " Fermi arc " which connects the points M to $-M$ given by the largest contour . Since the momentum in the z direction is not conserved, we can plot the projected contours on the surface $z = 0$. We consider the contour plot for different intensities $|S_{f^{(L,\sigma=\uparrow)},i}|^2(k_x, k_y)$ as a function of the momentum \vec{k} for a fixed valence band dispersion energy ϵ and spin polarization $\sigma = \uparrow$. We use the *contour plot program* where the " Fermi arc " is given by the contour plot $|S_{f^{(L,\sigma=\uparrow)},i}|^2(k_x, k_y) = 0$ representing the scattering intensity at a fixed energy. Such a contour connects the points M to $-M$. In practice, we can plot only contours which are close to zero. The lowest intensity contour is $|S_{f^{(L,\sigma=\uparrow)},i}|^2(k_x, k_y) = \text{constant} \cdot 10^{-7}$, which represents the largest contour. The rest of the contours correspond to increasing intensities. $|S_{f^{(L,\sigma=\uparrow)},i}|^2(k_x, k_y) = \text{constant} \cdot 2 \cdot$

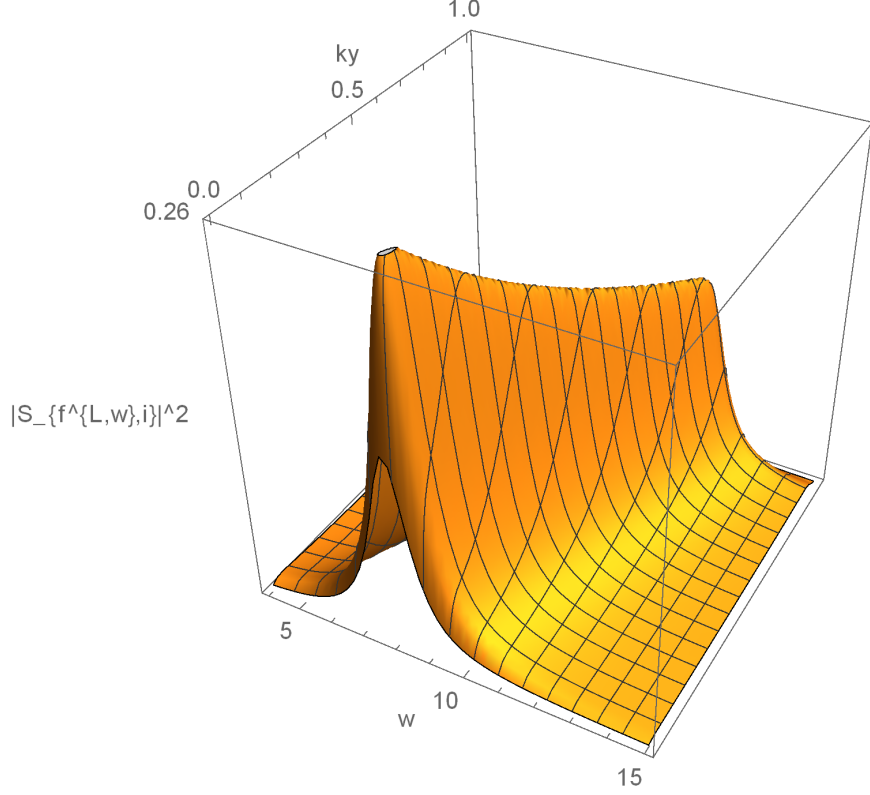


FIG. 2: The scattering intensity $|S_{f^{L,\sigma\uparrow},i}|^2(k_y, \Omega)$ as a function of the photon frequency Ω and the momentum k_y . (In figure 2 we have used the symbol W for the frequency Ω .) The confinement potential is $V_0 = 4ev$. The coordinates (x, y) corresponds to (k_y, Ω) , the z axis is represented by $|S_{f^{L,\sigma\uparrow},i}|^2(k_y, \Omega)$ computed for a small value of the life time Γ .

10^{-7} , $|S_{(f^{L,\sigma=\uparrow}),i}|^2(k_x, k_y) = \text{constant} \cdot 3 \cdot 10^{-7}$ and $|S_{f^{L,\sigma=\uparrow},i}|^2(k_x, k_y) = \text{constant} \cdot 4 \cdot 10^{-7}$, $|S_{(f^{L,\sigma=\uparrow}),i}|^2(k_x, k_y) = \text{constant} \cdot 5 \cdot 10^{-7}$, $|S_{f^{L,\sigma=\uparrow},i}|^2(k_x, k_y) = \text{constant} \cdot 6 \cdot 10^{-7}$, $|S_{(f^{L,\sigma=\uparrow}),i}|^2(k_x, k_y) = \text{constant} \cdot 7 \cdot 10^{-7}$, $|S_{f^{L,\sigma=\uparrow},i}|^2(k_x, k_y) = \text{constant} \cdot 8 \cdot 10^{-7}$. The plots are for a fixed energy $\epsilon(\vec{k}) = 100ev$. The *constant* in the contour plot originates from the proportionality factor $|M(\vec{k}, \Delta(\vec{k}), \vec{q}, \kappa)|^2$ in Eq.(20).

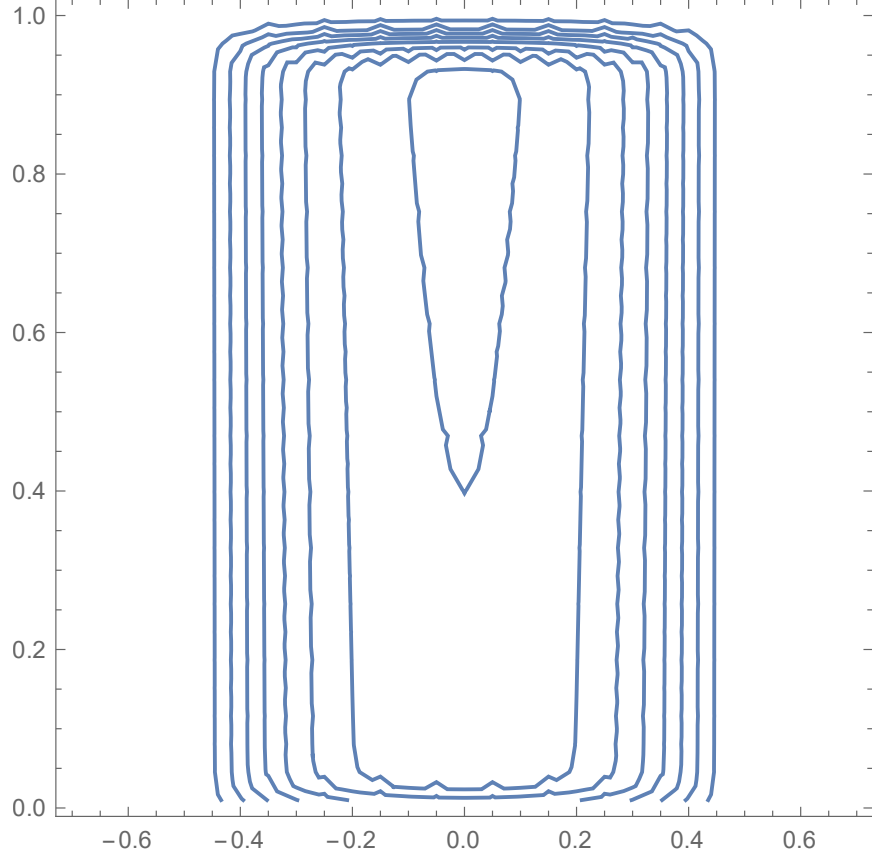


FIG. 3: The intensity contour as a function of k_x, k_y (horizontal and vertical axes). We plot the set solutions of the equation $|S_{f(L, \sigma=\uparrow), i}|^2(k_x, k_y) = \text{constant} \cdot 10^{-7}$ (the larger contour) will correspond to the " Fermi arc ". $|S_{f(L, \sigma\uparrow), i}|^2(k_x, k_y) = \text{constant} \cdot 8 \cdot 10^{-7}$ (the smallest contour) is depicted in ascending order for a fixed energy $\epsilon = 100ev$.

The intensity contour plot for $|S_{f(L,\sigma=\downarrow),i}|^2(k_x, k_y)$ reveals the arcs which connect $k_x = 0.5$ to $k_x = -0.5$ (shown in the figure 3) and arcs which start at $k_x = \pm 0.5$ and go to large momentum $k_x = \pm\infty$ which have opposite curvature (not shown).

By repeating the calculation for the final state $|f^{(R,\sigma)}\rangle$, we can obtain the scattering amplitude for the valence band energy $\hbar v(k_y - k_0)$.

The natural question which one can ask is what is the effect of the bulk electrons and how can they be detected? The bulk electrons have a non-relativistic dispersion contrary to the Weyl fermions. To detect the bulk electrons we need to consider the scattering matrix for the non-relativistic Hamiltonian $\vec{A} \cdot \vec{p}$ following the standard theory for photoemission [1]. This leads us to suggest that a realistic model for the *WSM* needs to contain both, linear dispersion for the Dirac like bands and parabolic dispersion for the bulk bands. The two contributions are additive and can be handled independently. According to the discussion in section IV the non-relativistic amplitude $S_{f(\text{parabolic},\sigma),i}$ needs to be computed and included in the scattering intensity must be given as $\approx \sum_{\sigma\uparrow,\downarrow} \left(|S_{f(R,\sigma),i}|^2 + |S_{f(L,\sigma),i}|^2 + |S_{f(\text{parabolic},\sigma),i}|^2 \right)$. The amplitudes will have complimentary contributions, the region $\epsilon = \hbar v(\pm k_y - k_0)$ and $\epsilon' = \frac{\hbar^2}{2m} |\vec{k}'|^2 - V_0$ correspond to different energies.

VI. The electron-electron interaction effects on the chiral modes which propagate on the boundary

In order to take into account the relaxations and screening on the boundary state electrons and holes we have to consider the Coulomb interactions. The first step is to project the electron operator $\hat{\Psi}_{\sigma,\tau_0}(\vec{k}, z)$, where $\sigma = \uparrow, \downarrow$ and $\tau_0 = 1, 2$ into the chiral modes given in Eqs.(6,9).

$$\begin{aligned}
\Psi_{\sigma=\uparrow,\tau_0=1}(\vec{x}, z) &= \\
&\int \frac{d^2k}{(2\pi)^2} \sqrt{2\hat{g}s(k_x)} e^{\hat{g}s(k_x)z} e^{i\vec{k}\cdot\vec{x}} \left[\frac{i}{2} \left(C_{R,-}(\vec{k}) + C_{L,-}(\vec{k}) \right) \alpha_-(k_x) - \frac{i}{2} \left(C_{R,+}(\vec{k}) + C_{L,+}(\vec{k}) \right) \alpha_+(k_x) \right] \\
\Psi_{\sigma=\downarrow,\tau_0=1}(\vec{x}, z) &= \\
&\int \frac{d^2k}{(2\pi)^2} \sqrt{2\hat{g}s(k_x)} e^{\hat{g}s(k_x)z} e^{i\vec{k}\cdot\vec{x}} \left[\frac{-1}{2} \left(C_{R,-}(\vec{k}) - C_{L,-}(\vec{k}) \right) \alpha_-(k_x) - \frac{1}{2} \left(C_{R,+}(\vec{k}) - C_{L,+}(\vec{k}) \right) \alpha_+(k_x) \right] \\
\Psi_{\sigma=\uparrow,\tau_0=2}(\vec{x}, z) &= \\
&\int \frac{d^2k}{(2\pi)^2} \sqrt{2\hat{g}s(k_x)} e^{\hat{g}s(k_x)z} e^{i\vec{k}\cdot\vec{x}} \left[\frac{i}{2} \left(C_{R,+}(\vec{k}) - C_{L,+}(\vec{k}) \right) \alpha_+(k_x) + \frac{i}{2} \left(C_{R,+}(\vec{k}) - C_{L,-}(\vec{k}) \right) \alpha_-(k_x) \right] \\
\Psi_{\sigma=\downarrow,\tau_0=2}(\vec{x}, z) &=
\end{aligned}$$

$$\int \frac{d^2k}{(2\pi)^2} \sqrt{2\hat{g}s(k_x)} e^{\hat{g}s(k_x)z} e^{i\vec{k}\cdot\vec{x}} \left[\frac{1}{2} \left(C_{R,+}(\vec{k}) + C_{L,+}(\vec{k}) \right) \alpha_+(k_x) + \frac{1}{2} \left(C_{R,-}(\vec{k}) + C_{L,-}(\vec{k}) \right) \alpha_-(k_x) \right] \quad (21)$$

The interaction Hamiltonian is obtained with the help of the Poisson equation $\nabla^2 a_0(\vec{x}, z) = -J_0(\vec{x}, z)$ for the scalar potential a_0 and electronic density $J_0(\vec{x}, z)$. Using the momentum representation given in Eq.(7) with the projected spinors given in Eq.(21) we find:

$$J_0(\vec{q}, z) = \sqrt{2\hat{g}s(k_x)} e^{\hat{g}s(k_x)z} \sum_{s=\pm} \int \frac{d^2k}{(2\pi)^2} \left[C_{R,s}^\dagger(\vec{k}) C_{R,s}(\vec{k} - \vec{q}) + C_{L,s}^\dagger(\vec{k}) C_{L,s}(\vec{k} - \vec{q}) \right] \alpha_s(k_x) \alpha_s(k_x - q_x) \quad (22)$$

The Coulomb interaction emerges from the integration of the scalar field $a_0(\vec{x}, z)$, given in *Appendix B*.

As a result of the Coulomb interaction H^{e-e} the Hamiltonian H^\perp is replaced by \tilde{H}^\perp :

$$\tilde{H}^\perp = H^\perp + H^{e-e} \quad (23)$$

Computing the scaling dimension, we observe that the Hamiltonian H^{e-e} is a marginal operator. This we can see in the following way by introducing the ultraviolet cutoff Λ . We scale $\Lambda \rightarrow \frac{\Lambda}{s}$, with $s > 1$. The re-scaling of the cutoff is achieved by the transformation of the momentum, $k' = sk$, $p' = sp$, $q' = sq$ and frequency $\omega' = s\omega$. The scaling of the momentum induces the scaling for the operators $C'_{R,s}(\vec{k}') = s^{-\beta} C_{R,s}(\vec{k})$, $C'_{L,s}(\vec{k}') = s^{-\beta} C_{L,s}(\vec{k})$ [22]. In addition, we need to check the scaling of $\alpha_+(k_x)$ and $\alpha_-(k_x)$. In the low momentum limit only $\alpha_-(k_x)$ remains invariant. Using scaling $k'_x = sk_x$ with $s > 1$ shows that if $k_x^2 < M^2$ the scaling relation is satisfied automatically $k_x^2 s^{-2} < M^2$. This will not be the case for $\alpha_+(k_x)$. The parameter $s(k_x) = \left| \left[\left(\frac{k_x}{M} \right)^2 - 1 \right] \right|$ is replaced under scaling by $s(k'_x) = \left| \left[\left(\frac{k_x}{Ms} \right)^2 - 1 \right] \right| \approx 1$ which can be taken in the long wave limit to be constant. This analysis simplifies the Hamiltonian in the long wave approximation replacing \tilde{H}^\perp with the long wave form H_{eff} .

$$\begin{aligned} H_{eff} = & \int \frac{d^2k}{(2\pi)^2} \left[\hbar v(k_y - k_0) C_R^\dagger(\vec{k}) C_R(\vec{k}) + \hbar v(-k_y - k_0) C_L^\dagger(\vec{k}) C_L \right] + \int \frac{d^2k}{(2\pi)^2} \int \frac{d^2p}{(2\pi)^2} \int \frac{d^2q}{(2\pi)^2} \\ & \cdot \left[C_R^\dagger(\vec{k}) C_R(\vec{k} - \vec{q}) + C_L^\dagger(\vec{k}) C_L(\vec{k} - \vec{q}) \right] V^e(|\vec{q}|) \left[C_R^\dagger(\vec{p}) C_R(\vec{p} + \vec{q}) + C_L^\dagger(\vec{p}) C_L(\vec{p} + \vec{q}) \right] \\ & + \int \frac{d^2k}{(2\pi)^2} W(k_x, \vec{q}) A_y(\vec{q}, t) \left[C_L^\dagger(\vec{k}) C_L(\vec{k} + \vec{q}) - C_R^\dagger(\vec{k}) C_R(\vec{k} + \vec{q}) \right] \\ W(k_x, \vec{q}) = & \frac{2\hat{g} e^{-i \tan^{-1} \left(\frac{q_z}{2\hat{g}} \right)}}{\sqrt{(2\hat{g})^2 + q_z^2}} \end{aligned} \quad (24)$$

The boundary surface for a two dimensional space gives rise to a $2 + 1$ scaling problem. The Hamiltonian H_0^\perp is scale invariant and fixes β to $\beta = -2$. As a result we find that the potential $V^c(|\vec{q}|) = \frac{e^2}{2\epsilon|\vec{q}|}$ is marginal, s^0 [22]. Our surface boundary model with interactions is in the same universality class as interacting graphene [19]. We find that the Coulomb potential is marginal irrelevant (see Appendix B) $V^c(|\vec{q}|) = \frac{\alpha_0}{2\epsilon|\vec{q}|}$. Due to renormalization effects the potential is replaced by: $V^c(|\vec{q}|) = \frac{\alpha_{eff}}{2|\vec{q}|}$, with $\alpha_{eff} = \alpha_0 \left(1 + \frac{\alpha_0}{4} Ln \frac{\Lambda}{T}\right)^{-1}$. We observe that the potential is vanishing logarithmically at low temperature, the velocity v and the life time Γ become temperature dependent:

$$v(T) = v \left(1 + \frac{\alpha_0}{4} Ln \frac{\Lambda}{T}\right), \Gamma(T) \approx \alpha_0^2 K_B T \quad (25)$$

VII. Conclusions

We have introduced a model for the *WSM* with two nodal points and a surface boundary at $z = 0$, giving rise to two chiral bands. The model uses a Hamiltonian which considers a non-linear function connecting the nodes. Using the minimal coupling principle, we couple the electrons to photons without relying on the Foldy-Wouthuysen transformation. Thus traditional non-relativistic coupling $\vec{A} \cdot \vec{p}$ is avoided allowing for an exact modeling of electrons and photons. The Coulomb interaction is expressed in terms of the chiral surface modes. We find that the projected interaction gives rise to a model which is in the same universality class as graphene in $2 + 1$ dimensions, resulting in a normalization of the velocity and the life time.

The main goal of this work is to introduce the S matrix for investigating photoemission. We find that our theory explains most of the experimental observations. The limitation of one band, two nodes versus many bands and nodes in a real *WSM* does not to change the photoemission profile. Our model reveals the special properties of the *WSM* observed experimentally. We theoretically compute the valence and conduction band dispersion for the chiral surface boundary and demonstrate the emergence of the "Fermi arcs". When the number of nodes is larger than two, such as in the *TaAs*, the methodology used in this paper can be applied by replacing the quadratic function $(k_x^2 - M^2)$ with a polynomial function $f(k_x)$ which has $2N$ zeros. This will give rise to multiple valence band dispersions for different crystal surfaces.

Appendix A

The Wick theorem reduces the T -product to a product of contractions (given by Green's function), then it acts on the uncontracted fields on the initial state $|i\rangle = A_r^\dagger(\vec{q})|0\rangle$ and final state $\langle f^{(L,\sigma=\uparrow)}|, \langle f^{(L,\sigma=\downarrow)}|$. For $\langle f^{(L,\sigma=\uparrow)}|$, Wick theorem generates the following result:

$$\begin{aligned}
S_{f^{(L,\uparrow)},i} &\propto \left(\frac{-i}{\hbar}\right)^2 \int_0^\infty \frac{dk_z}{\pi} M(\vec{k}, k_z, \vec{q}) \theta[-k_y] \theta[k_y + q_y] \int_{-\infty}^\infty dt \int_{-\infty}^\infty dt' (-i) \cdot \\
&\langle f^{(L,\sigma=\uparrow)}| \left(\theta[-M^2 + k_x^2] f_{\uparrow}^\dagger(\vec{k}, k_z; t) a_{L,s=-}(\vec{k}; t) a_{L,s=-}^\dagger(\vec{k}; t') b_{L,s=-}(-k_y - q_y; t') e^{-ih\Omega(\vec{q})t'} A_r(\vec{q}) \right) A_r^\dagger(\vec{q}) |0\rangle \\
&\propto \left(\frac{-i}{\hbar}\right)^2 \int_0^\infty \frac{dk_z}{\pi} M(\vec{k}, k_z, \vec{q}) \theta[-k_y] \theta[k_y + q_y] \theta[-M^2 + k_x^2] \int_{-\infty}^\infty dt \int_{-\infty}^\infty dt' \cdot \\
&\left(e^{-iE(\vec{k}, k_z)t} \langle T(a_{L,s=-}(\vec{k}; t) a_{L,s=-}^\dagger(\vec{k}; t')) \rangle e^{ihv(k_y+k_0+q_y)t'} e^{-ih\Omega(\vec{q})t'} \right)
\end{aligned} \tag{26}$$

From Wick theorem, we obtain the following the scattering amplitude for $\langle f^{(L,\sigma=\downarrow)}|$:

$$\begin{aligned}
S_{f^{(L,\downarrow)},i} &\propto \left(\frac{-i}{\hbar}\right)^2 \int_0^\infty \frac{dk_z}{\pi} M(\vec{k}, k_z, \vec{q}) \theta[-k_y] \theta[k_y + q_y] \int_{-\infty}^\infty dt \int_{-\infty}^\infty dt' \\
&\langle f^{(L,\sigma=\downarrow)}| \left(\theta[M^2 - k_x^2] f_{\downarrow}^\dagger(\vec{k}, k_z; t) a_{L,s=+}(\vec{k}; t) a_{L,s=+}^\dagger(\vec{k}; t') b_{L,s=+}(-k_y - q_y; t') e^{-ih\Omega(\vec{q})t'} A_r(\vec{q}) \right) A_r^\dagger(\vec{q}) |0\rangle \\
&\propto \left(\frac{-i}{\hbar}\right)^2 \int_0^\infty \frac{dk_z}{\pi} M(\vec{k}, k_z, \vec{q}, \kappa) \theta[-k_y] \theta[k_y + q_y] \theta[M^2 - k_x^2] \int_{-\infty}^\infty dt \int_{-\infty}^\infty dt' \cdot \\
&\left(e^{iE(\vec{k}, k_z)t} \langle T(a_{L,s=+}(\vec{k}; t) a_{L,s=+}^\dagger(\vec{k}; t')) \rangle e^{ihv(k_y+k_0+q_y)t'} e^{-ih\Omega(\vec{q})t'} \right)
\end{aligned} \tag{27}$$

Here the matrix element $M(\vec{k}, k_z, \vec{q}, \kappa)$ is given by the product of $W(\vec{k}, \vec{q})$ and $S(\vec{k}, k_z, \kappa)$ introduced in Eq.(8) and Eq.(13): $M(\vec{k}, k_z, \vec{q}, \kappa) = W(\vec{k}, \vec{q}) S(\vec{k}, k_z, \kappa) V_0 e_r^{(y)}(\vec{q})$.

Appendix B

We solve the Poisson equation. We integrate the scalar field $a_0(\vec{x}, z)$ and find:

$$\begin{aligned}
H^{int.C} &= \\
&\int \frac{d^2q}{(2\pi)^2} \int \frac{dq_z}{2\pi} \left[\frac{1}{2\epsilon e^2} a_0(\vec{q}, q_z) \left(q_x^2 + q_y^2 + q_z^2 \right) a_0(-\vec{q}, -q_z) + a_0(\vec{q}, q_z) \left(\int_{-L}^0 dz \sqrt{2\hat{g}s(k_x)} e^{(\hat{g}s(k_x)+iq_z)z} \right) \right. \\
&\cdot \left. \sum_{s=\pm} \int \frac{d^2k}{(2\pi)^2} \left(C_{R,s}^\dagger(\vec{k}) C_{R,s}(\vec{k} - \vec{q}) + C_{L,s}^\dagger(\vec{k}) C_{L,s}(\vec{k} - \vec{q}) \right) \alpha_s(k_x) \alpha_s(k_x - q_x) \right]
\end{aligned} \tag{28}$$

The scalar field correlation is given by the longitudinal Coulomb propagator $D_0(\vec{q}, q_z) = \frac{e^2}{2\epsilon(q_z^2 + q_y^2 + q_x^2)}$. The integration with respect to the k_z momentum in the presence of the second

term in Eq.28 and the long wave limit $s(k_x) \approx 1$ gives the effective surface potential $V^c(|\vec{q}|)$:

$$V^c(|\vec{q}|) = \int \frac{dq_z}{2\pi} \frac{2e^2}{\epsilon(q_x^2 + q_y^2 + q_z^2)} \cdot \frac{1}{1 + \frac{q_z^2}{2\hat{g}}} \approx \frac{e^2}{2\epsilon|\vec{q}|} + \frac{e^2}{2\pi\epsilon} \cdot \frac{\Lambda}{2\hat{g}} \left[1 + \frac{|\vec{q}|}{\Lambda} \text{Ln}\left(\frac{|\vec{q}|}{\Lambda}\right) \dots \right] \quad (29)$$

where $V^c(|\vec{q}|)$ is marginal and the higher order terms give irrelevant contributions [22]. The correction term $\frac{\Lambda}{2\hat{g}}$ will give rise to a shift of the crystal -vacuum potential V_0 introduced in Eq.(2). This strength of the interactions is characterized by $\alpha_0 = \frac{1}{137} \frac{c}{\epsilon_r v}$ where $\epsilon_0 \epsilon_r$ is the dielectric constant. The leading order potential is given by $V^c(|\vec{q}|) = \frac{\alpha_0}{2|\vec{q}|}$.

-
- [1] G.D.Mahan, Phys.Rev.Lett. **24**,1068 (1970)
 - [2] E. Witten, arXiv :cond-mat/1510.07698 and Reviews of Modern Physics **88**,035001 (2016) see Eq.(3.12) on page 035001 -23.
 - [3] H. Weyl, Z.Phys.**56** 330 (1929).
 - [4] X. Wan, A.M. Turner, A. Vishwanath, and S.Y.Savrasov, Phys.Rev.B. **83**, 205101 (2011).
 - [5] G.Xu,H.Weng,Z.Wang,X.Dai and Z.Fang ,Phys.Rev.Lett. **107**, 186806 (2011).
 - [6] H.Nielsen and M.Ninomiya,Phys.Lett. B **130**, 389 (1983).
 - [7] D.T.Son and B.Z.Spivak, Phys.Rev.B **88**,104412 (2013)
 - [8] D.T. Son and N.Yamato, Phys.Rev.Lett. **109**, 181602 (2012).
 - [9] Su-Yang Xu, Ilya Belopolski,Nasser Alidoust, Madhab Neupaine, Guang Bian, Chenglong Zhang, Raman Sankar, Guoqing Chang, Zhujun Yuan, Chi-Cheng Lee, Shin-Ming Huang, Hao Zheng, Jie Ma, Daniel S.Sanchez, BaoKai Wang, Arun Bansil, Fangcheng Chou, Pavel P.Shibayev, Hsin Lin, Shuang Jia, M.Zahid Hasan Science, vol. 349 ISSUE 6248 (2015)
 - [10] B.Q. Lv, H.M. Weng, B.B.Fu, X.P. Wang, H.Miao, J.Ma, P.Richard, X.C. Huang, L.X. Zhao, G.F. Chen, Z.Fang, X.Dai, T. Qian, and H.Ding, Phys. Rev.Lett. **115** 217601 (2015)
 - [11] Rajib Batabyal,Noam Morali, Nurit Avraham, Yan Sun, Marcus Schmidt, Claudia Felser, Ady Stern, Binghai Yan, Haim Beidenkopf, Sci. Adv. **2**, e1600709 (2016).
 - [12] Guoqing Chang, Su-Yang Xu, Hao. Zheng,Chin-Cheng Lee, Shin-Ming Huang, Ilya Belopolski, Daniel S. Sanchez, Guang Bian, Naser Alidoust, Tay-Rong Chang,Chuang -Han Hsu, Horn-Tay Jeng, Arun Bansil, Hsin Lin ,and M.Zahid Hasan, Phys.Rev.Lett. **116**, 066601 (2016)

- [13] S. Kourtis, Jian Li, Zhijun Wang, Ali Yazdani, B.Andrei Bernevig, Phys. Rev. B **93**, 041109(R) (2016)
- [14] Adolpho G.Grushin, Teemu Ojanen and Jens H.Badarson Phys.Rev. B **93**, 075114 (2016)
- [15] Chiang, T.C. Knapp, J.A.Aono, M. Eastman, D.E. Phys.Rev.B **21**, 3513 (1980)
- [16] Michael E.Peskin and Daniel Schroeder ” An introduction to Quantum Field Theory”, Copyright 1995 by Westview Press.
- [17] L.L. Foldy and S.A. Wouthuysen , Phys. Rev. **78**,29 (1950).
- [18] Xiao-Liang Qi and Shou-Cheng Zhang ,Rev.Mod. Phys. **83**, 1057 (2011)
- [19] Andrew Lucas, Jesse Crossno, Kim Chung Fong, Philip Kim,and Subir Sachdev Phys. Rev. B **93**,075426 (2016)
- [20] D.T. Son Phys.Rev.B **75**, 235423 (2007).
- [21] Shinobu Hikami, Phys. Rev. B**24**, 2671 (1981).
- [22] R.Shankar Rev.Mod. Phys. vol **68**,No.1 ,157 (1994)